JOURNAL OF GUIDANCE, CONTROL, AND DYNAMICS
Vol. 23, No. 3, May–June 2000

Evaluation of the Dynamic Environment of an Asteroid: Applications to 433 Eros

D. J. Scheeres*
University of Michigan, Ann Arbor, Michigan 48109-2140
and
B. G. Williams† and J. K. Miller‡
Jet Propulsion Laboratory, California Institute of Technology, Pasadena, California 91109

Methods of analysis to quickly and systematically evaluate the dynamical environment close to an asteroid are presented, concentrating on the effect of the asteroid's gravity field and rotation state on a spacecraft orbit. Such an analysis is useful and needed for missions to small solar system bodies such as asteroids and comets, where the true mass, gravity field, and rotation state will not be known until after the spacecraft rendezvous with the body and these quantities are estimated. Generally, after these quantities have been estimated, the complete mission profile must be redesigned in accordance with the actual values found at the asteroid. An integral part of this redesign is the characterization of dynamics close to the asteroid, specifically the computation of orbit stability close to the body and the practical limits on how close the spacecraft can fly to the body before large perturbations are experienced. Numerical computations of such an evaluation applied to the asteroid 433 Eros, the target of the Near Earth Asteroid Rendezvous (NEAR) mission, using preliminary models of the asteroid obtained during NEAR's December 1998 flyby of Eros are presented.

I. Introduction

THE prospect of orbital missions to asteroids and comets has opened the door on a new and fruitful area of research in astrodynamics: the study and quantification of the stability and navigability of spacecraft orbits in close proximity to rotating, irregularly shaped bodies. This area of study is challenging because each new body has its own peculiarities in terms of size, shape, density, and rotation state, and complicated because these quantities are often not known until after the spacecraft has its rendezvous with the body. Thus, preencounter mission and navigation plans must always be kept flexible and general enough to accommodate a wide range of possible body parameters. To enable a relatively rapid mission and navigation design once the spacecraft arrives at the body requires that systematic approaches to the characterization and evaluation of the orbital dynamics about asteroids be formulated prior to encounter. In this paper we present some results that allow such a characterization to be performed and apply them to the estimated mass, shape, and rotation state of asteroid 433 Eros, the target asteroid of the Near Earth Asteroid Rendezvous (NEAR) mission. The same procedures outlined here are also applicable to any arbitrary body in uniform rotation, the extension of the characterization process to bodies in nonuniform rotation being significantly different.[1]

The specific issues focused on are the computation of orbit stability limits about uniformly rotating bodies. We will investigate both analytical formulas with which to express the perturbation felt by a spacecraft orbit and specific numerical computations that can be performed to establish stability limits. Our ultimate goal is to combine these two modes of analysis into a single systematic approach to understanding and evaluating the dynamic environment about an asteroid or comet. The current analysis rests on a series of previous analyses made of the problem of orbiting a comet or asteroid.[2–7] This paper synthesizes these previous results and extends them to practical mission applications for a spacecraft.

Received 25 March 1999; revision received 1 October 1999; accepted for publication 8 October 1999.

*Assistant Professor, Department of Aerospace Engineering, 3048 FXB; scheeres@umich.edu. Senior Member AIAA.
†Group Supervisor, Navigation and Flight Mechanics Section. Member AIAA.
‡Senior Member of Engineering Staff, Navigation and Flight Mechanics Section. Associate Fellow AIAA.

II. Model Definition

To evaluate the dynamics of a spacecraft close to an asteroid requires a description of the gravitational field of the asteroid and its rotational state. Both of these items can be obtained following rendezvous with the target asteroid by reducing radiometric tracking data, optical images of the asteroid, and any other measurements that may be available.[8] This model and parameter estimation is the first order of business and must be performed prior to the detailed design of close-proximity operations.

For numerical computations in this paper we use the preliminary model of asteroid 433 Eros, obtained during the December 1998 flyby of that asteroid by the NEAR spacecraft. Thus, this paper presents a case study that can be used to aid the design of the NEAR spacecraft orbital mission about Eros.

A. General Asteroid Model

The general model for a uniformly rotating asteroid consists of a rotation period and a gravity field. Because of internal dissipation forces that act on rotating asteroids, they eventually relax into a uniform rotation about their largest moment of inertia regardless of their initial rotational state. For most asteroids with rotation periods of a day or less, the time for this relaxation to occur is relatively short in terms of solar system time-scales.[9,10] Thus, the majority of asteroids are believed to be in or close to a uniform rotation state, and this justifies our restriction to this case.

The standard gravity field model used for navigation operations about a small body is the spherical harmonic expansion field, which can be estimated from the radiometric data, combined with optical data to fix the relative orientation of the asteroid with respect to the spacecraft. The usual specification of this field is truncated at some degree and order and is expressed as

$$U = \frac{\mu}{r}\sum_{i=0}^{N}\sum_{j=0}^{i}\left(\frac{R_0}{r}\right)^i P_i^j(\sin\delta)[C_{ij}\cos(j\lambda) + S_{ij}\sin(j\lambda)] \quad (1)$$

where μ is the asteroid mass times the universal gravitational constant; R_0 is the normalizing radius, usually taken as either the radius of the circumscribing sphere about the asteroid or the mean volumetric radius; P_i^j is the associated Legendre function; C_{ij} and S_{ij} are the spherical harmonic gravity coefficients, and r, δ, and λ are the radius, latitude, and longitude coordinates, respectively, of the spacecraft in the asteroid fixed frame. For the NEAR mission,

$N = 16$ is the highest degree and order of the harmonic expansion that will be used.[8] Usually, the gravity field is expanded about the center of mass of the asteroid, yielding $C_{1j} = S_{11} = 0$, and with its coordinate axes oriented so that they lie along the principal axes of inertia, yielding $C_{21} = S_{21} = S_{22} = 0$.

The spherical harmonic gravity field is the best descriptor of the asteroid gravity field when outside of the circumscribing sphere about the asteroid (the circumscribing sphere is the sphere of minimum radius that contains the asteroid, centered at the expansion center of the gravity field). When inside of this sphere, the spherical harmonic expansion field may diverge and no longer yield accurate information about the true gravity field. For the case of an ideal ellipsoid, the harmonic expansion will diverge if the ratio of the largest and smallest dimensions of the ellipsoid is greater than $\sqrt{2}$ (Ref. 11). This same result is seen to hold, approximately, for irregular shapes that are roughly ellipsoidal in shape. For Eros, the ratio of maximum to minimum dimension is approximately 2.3, much larger than the divergence limit, and indicative that the gravity field will likely diverge when near the surface.[12]

For most orbital applications, this divergence is not of great concern because the spacecraft will normally remain outside of this circumscribing sphere. For situations in which a landing or extremely close pass over the asteroid surface is desired, however, this divergence will affect the design, prediction, and control of the spacecraft orbit. In these situations it is necessary to specify the asteroid gravity field using a formulation that does not diverge. There are several different approaches to this problem; the one which we use here is based on modeling the gravity field of the asteroid as the summation of gravity fields of tetrahedra, for which a closed-form formula is known.[12,13]

For the purposes of the analysis, both the harmonic expansion field and the tetrahedron field will be used, the integrating software switching from one gravity field specification to the other when crossing through a sphere slightly larger than the circumscribing sphere. To ensure equality of the two fields, the harmonic expansion will be computed using the shape model and a constant density assumption,[12] an approach that has been applied previously.[1,5]

In addition to the gravity and rotation models, it is also important to incorporate the perturbations from the sun in any detailed analysis of the motion of a spacecraft about an asteroid. There are two main contributions from the sun: gravity and radiation pressure. The effect of the solar gravity becomes pronounced as the distance of the spacecraft from the asteroid increases. Generally, at some point the solar gravity dominates the spacecraft dynamics, and the nature of motion changes from simple orbital motion about a central body. The radiation pressure from the sun has a constant direction and magnitude at a given distance of the asteroid from the sun. Again, the effect of this force becomes more pronounced as the spacecraft flies farther away from the asteroid. We will assume that the spacecraft will remain close to the central body, reducing the solar effects to small perturbations. As a result, they will not be accounted for in this analysis.

B. Specific Model of 433 Eros

On 23 December 1998, the NEAR spacecraft had a close flyby of asteroid 433 Eros, simultaneously imaging the asteroid and tracking the spacecraft. Resulting from these images and tracking data are estimates of the asteroid shape and overall mass, two key parameters that can be used to generate the models needed for computation in this paper.

The mass estimate of the asteroid was computed and yielded an estimated value of the gravitational parameter:

$$\mu = 5 \times 10^{-4} \text{ km}^3/\text{s}^2 \tag{2}$$

with formal error of 1×10^{-4}, $1-\sigma$. This large error was due to the distance of the flyby (4000 km) and the relative speed between the spacecraft and asteroid (1 km/s). Thus, the computations given in this analysis must be treated as uncertain and cannot be made more accurate until the NEAR spacecraft has its rendezvous with Eros (currently scheduled to occur in February 2000).

The shape model of Eros was obtained from the NEAR Multispectral Imager science team[14] and has a 5-deg surface resolution. It has a total estimated volume of approximately 3000 km^3 and a mean (volumetric) radius of 8.97 km. This shape will also be refined following the NEAR spacecraft rendezvous with the asteroid.

We have transformed the shape model into a triangular plate model with 2432 vertices and 4860 plates, centered it at its volumetric center, and oriented it along its principal axes of inertia (assuming constant density). We compute the constant density gravitational field coefficients corresponding to the given shape.[15] Of particular interest are the second-degree and order gravity field coefficients C_{20} and C_{22}:

$$R_0^2 C_{20} = -26.755 \text{ km}^2 \tag{3}$$

$$R_0^2 C_{22} = 12.752 \text{ km}^2 \tag{4}$$

In our analytical section we will normally take $R_0 = 1$ because it is an arbitrary constant, hence specifying the coefficients C_{20} and C_{22} as dimensional. These particular values of the gravity field will be used extensively in our analysis, as well as the full gravity field computed from the shape model.

Finally, for the Eros rotation period we use a value of 5.27 h. This estimate is based on ground-based observations of Eros using both optical and radar imaging and is considered to be extremely well known.[16] The rotation rate of the asteroid is denoted as ω_T.

C. Equations of Motion

Having discussed in detail the main perturbations acting on a spacecraft close to an asteroid, we can state the general equations of motion in this frame. There are two forms of the equations of motion that are useful for our analysis. The first states the equations in the body-fixed frame, a frame with uniform rotation. In this coordinate system the central gravity field does not change with time and, because the rotational rate of the asteroid does not change either, the equations of motion are time invariant.

In the body-fixed reference frame the equations of motion are

$$\ddot{x} - 2\omega_T \dot{y} = \omega_T^2 x + U_x \tag{5}$$

$$\ddot{y} + 2\omega_T \dot{x} = \omega_T^2 y + U_y \tag{6}$$

$$\ddot{z} = U_z \tag{7}$$

Because these equations are time invariant, an additional integral of motion exists (termed the Jacobi constant) and is

$$J = \tfrac{1}{2}(\dot{x}^2 + \dot{y}^2 + \dot{z}^2) - \tfrac{1}{2}\omega_T^2 (x^2 + y^2) - U \tag{8}$$

The Jacobi integral can be used to derive sharp limits on when a spacecraft cannot impact with the asteroid surface, providing a degree of safety for some types of orbital operations.

An alternate description of the orbit dynamics is found using a special subset of the Lagrange planetary equations. These equations express the change in orbital elements, or other integrals of motion of the Kepler problem, as a function of perturbing forces acting on the spacecraft. These equations are generally not convenient for numerical computation in an asteroid system, but are useful for the development of analytic approximations to evaluate the effect of the rotating gravity field on the orbiting spacecraft.

For our computations it is useful to use the canonical form of the Lagrange equations[17] that express the change in orbit Keplerian energy, angular momentum, and angular momentum projected onto the z axis as a function of the gravitational perturbations acting on them. The equations describing these changes can be expressed as

$$\frac{dC}{dt} = \frac{\partial R}{\partial t} \tag{9}$$

$$\frac{dG}{dt} = \frac{\partial R}{\partial \omega} \tag{10}$$

$$\frac{dH}{dt} = \frac{\partial R}{\partial \Omega} \tag{11}$$

where

$$C = -\mu/2a \tag{12}$$

$$G = \sqrt{\mu a(1-e^2)} \tag{13}$$

$$H = G\cos i \tag{14}$$

$$R = U - \mu/r \tag{15}$$

and a, e, i, ω, and Ω are the osculating orbital elements. Equations (10) and (11) are taken from classical results,[17] whereas Eq. (9) is derived by applying the chain rule, taking the partial of R with respect to the true anomaly f first and then taking the partial of the true anomaly f with respect to the time.[5] Note that we neglect to add the additional equations describing the dynamics of the argument of periapsis, longitude of the ascending node, and mean epoch because we will not explicitly study those equations here.

It is important to restate the Jacobi integral in terms of the variables considered here. In this system the integral takes on a particularly simple form when so evaluated:

$$J = C - \omega_T H - R \tag{16}$$

where ω_T is again the rotation rate of the asteroid, C is the Keplerian energy, H is the angular momentum projected onto the z axis, and R is the perturbing potential.

III. Analytic Characterization

First we describe the application of approximate, analytical analysis to characterize spacecraft orbital dynamics about a uniformly rotating body. The results from such an analysis are not as exact as our numerical computations, but have general application because several key parameters can be left in functional form. There are two basic analytic characterizations that can be performed, both involving terms from the second-degree and order gravity field.

A. Effect of Asteroid Oblateness

The effect of the C_{20} gravity term, or the oblateness, on a spacecraft orbit has been studied extensively in connection with the Earth orbiter problem.[18–20] To accurately capture this effect analytically requires the inclusion of higher-order gravity terms, such as C_{40}. The relevant items for this analysis are the secular rates in argument of periapsis, the longitude of ascending node, and the mean anomaly. The leading terms of that analysis are

$$\frac{\mathrm{d}\bar{\omega}}{\mathrm{d}t} = \frac{3nC_{20}}{2p^2}\left(\frac{5}{2}\sin^2 i - 2\right) \tag{17}$$

$$\frac{\mathrm{d}\bar{\Omega}}{\mathrm{d}t} = \frac{3nC_{20}}{2p^2}\cos i \tag{18}$$

$$\bar{n} = n\left[1 + \frac{3C_{20}\sqrt{1-e^2}}{2p^2}\left(\frac{3}{2}\sin^2 i - 1\right)\right] \tag{19}$$

Note that the secular rates of these angles can become very large when orbiting close to asteroids. The leading frequency of these variations, $A_{20} = 3nC_{20}/(2p^2)$, can be computed for Eros to be

$$A_{20} = -85.6\left[1\Big|\ \tilde{a}^{\frac{7}{2}}(1-e^2)^2\right] \text{ deg/h} \tag{20}$$

where $\tilde{a}$ is the spacecraft semimajor axis normalized by the mean asteroid radius (8.97 km for Eros) and e is the orbital eccentricity. The corresponding frequency for an Earth orbiter is 0.415 deg/h. Thus, for operations within several mean radii of the asteroid, the spacecraft orbit will be subject to large secular rates in its orbit-plane orientation and in-plane orientation.

Once an orbit is chosen that is safe from most destabilizing influences, such as a retrograde orbit, these large secular rates must still be accounted for and cannot, except in a few specific orbit geometries, be directly controlled. The impact and control of these effects have been evaluated for the NEAR orbital mission plan.[4]

B. Effect of Asteroid Ellipticity

Although the effect of a large asteroid oblateness has been classically characterized, the effect of a large asteroid ellipticity has not been closely studied. The difficulties encountered in studying the effect of this term are due to the time-varying nature of the interaction between asteroid and spacecraft. For a terrestrial planet where the ellipticity is in general small, these effects can be partly characterized by simple averaging theories.[21] At asteroids where these ellipticities can approach 0.8 and even higher, however, classical analyses fail.

For asteroids this effect has been studied numerically in the literature,[2–6] where it has been clearly established that, due to interaction of a spacecraft orbit with the asteroid ellipticity, the spacecraft orbit can transition from a seemingly safe orbit into an impacting or escaping orbit within a few orbit periods. There are a variety of ways in which this effect can be studied; a later section investigates the effect by computing equilibrium points and periodic orbits and evaluating their stability. In this section we present a new approach to the analysis[6,7] that gives explicit predictions of the effect of the main component of the asteroid ellipticity, the C_{22} gravity term, on a spacecraft orbit.

The force potential due to the C_{22} gravity term is

$$U_{22} = (3\mu/r^3)C_{22}\cos^2\delta\cos(2\lambda) \tag{21}$$

where δ is the spacecraft declination in the body-fixed frame and λ is the body-fixed longitude. Expanding the potential in terms of osculating orbit elements yields

$$\begin{aligned} U_{22} = \left(3\mu C_{22}\Big|\ r^3\right)\Big[&\tfrac{1}{2}\sin^2 i\,\{\cos 2\Omega\cos 2\omega_T t + \sin 2\Omega\sin 2\omega_T t\} \\ &+ \cos^4(i/2)\{\cos 2(\omega+\Omega)\cos 2(f-\omega_T t) \\ &- \sin 2(\omega+\Omega)\sin 2(f-\omega_T t)\} \\ &+ \sin^4(i/2)\{\cos 2(\omega-\Omega)\cos 2(f+\omega_T t) \\ &- \sin 2(\omega-\Omega)\sin 2(f+\omega_T t)\}\Big] \end{aligned} \tag{22}$$

where the body-fixed and inertial coordinate frames are assumed to be aligned at time $t = 0$.

To evaluate the effect of the C_{22} term over one orbit, integrate over Eqs. (10) and (11), treating all of the orbit elements as constant and only allowing the time and true anomaly to vary. We integrate over one encounter, from apoapsis to apoapsis, choosing the orbital elements of ω and Ω such that they are fixed at their periapsis values, which at $t = 0$ corresponds to these elements being specified in the body-fixed frame:

$$\Delta G = \int_{-T/2}^{T/2} \frac{\partial R}{\partial \omega}\,\mathrm{d}t \tag{23}$$

$$\Delta H = \int_{-T/2}^{T/2} \frac{\partial R}{\partial \Omega}\,\mathrm{d}t \tag{24}$$

The corresponding change in the orbit energy, ΔC, can be directly solved for from the Jacobi integral, Eq. (16):

$$\Delta C = \omega_T \Delta H + U_{22}(f=\pi) - U_{22}(f=-\pi) \tag{25}$$

Evaluation of these equations yields the results

$$\begin{aligned} \Delta G = -6C_{22}\sqrt{\mu/p^3}\Big[&\cos^4(i/2)\sin 2(\omega+\Omega)I_2^1 \\ &+ \sin^4(i/2)\sin 2(\omega-\Omega)I_{-2}^1\Big] \end{aligned} \tag{26}$$

$$\begin{aligned} \Delta H = -6C_{22}\sqrt{\mu/p^3}\Big[&\tfrac{1}{2}\sin^2 i\sin 2\Omega I_0^1 + \cos^4(i/2) \\ &\times \sin 2(\omega+\Omega)I_2^1 - \sin^4(i/2)\sin 2(\omega-\Omega)I_{-2}^1\Big] \end{aligned} \tag{27}$$

$$\begin{aligned} \Delta C = -6C_{22}\omega_T\sqrt{\mu/p^3}\Big[&\tfrac{1}{2}\sin^2 i\sin 2\Omega\left\{I_0^1 - (1-e)^3 I_0^{-2}\right\} \\ &+ \cos^4(i/2)\sin 2(\omega+\Omega)\left\{I_2^1 - (1-e)^3 I_0^{-2}\right\} \\ &- \sin^4(i/2)\sin 2(\omega-\Omega)\left\{I_{-2}^1 - (1-e)^3 I_0^{-2}\right\}\Big] \end{aligned} \tag{28}$$

where the integrals I_m^n have the definition

$$I_m^n = \int_{-\pi}^{\pi} (1 + e\cos f)^n \cos(mf - 2\omega_T t)\,\mathrm{d}f \tag{29}$$

These integrals cannot be expressed in closed form in general except for the particular case

$$I_0^{-2} = \frac{\sin\left(2\pi\sqrt{\omega_T^2 a^3/\mu}\right)}{\sqrt{\omega_T^2 p^3 \mu}} \tag{30}$$

The numerical quadrature of these integrals has been treated previously.[7]

These integrals express how the spacecraft true anomaly rate interacts with the asteroid rotation rate and, in general, have a complicated form. The values of these integrals are best presented as contour plots as a function of nominal orbit periapsis radius and eccentricity. Figures 1 and 2 show the contour values of the integrals I_2^1 and I_{-2}^1 for comparison. We see that, in general, $I_2^1 \gg I_{-2}^1$ in the region that interests us. Similarly, we find that $I_2^1 \gg I_0^1$. Several important insights are immediately obtained on inspection of the contour plots and the functional form of Eqs. (26–28). Most important, direct, low-inclination orbits will be subject to the terms I_2^1, whereas retrograde, near equatorial orbits will be primarily subject to the terms I_{-2}^1. By the inspection of the contour plots, it is obvious that direct orbits will experience much larger changes in energy and angular momentum for each orbit, whereas the retrograde orbits will experience little, if any, change per orbit. This result explicitly predicts the relative stability of retrograde orbits noticed previously in the literature[2–5] and predicts the large variations in energy and angular momentum in a concise and clear fashion. In the following we will neglect I_{-2}^1 and I_0^1 to gain a simpler form for Eqs. (26–28).

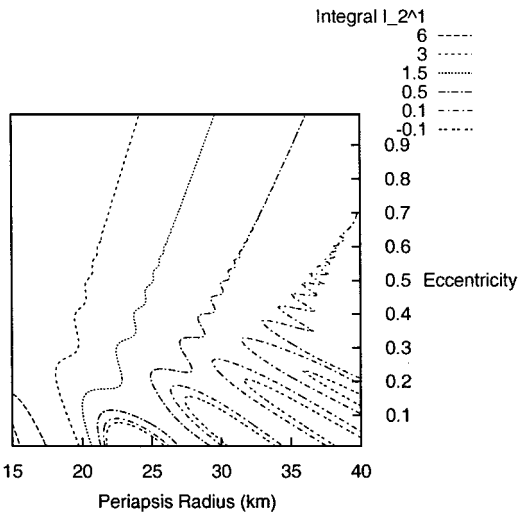

Fig. 1 Contour plot of integral I_2^1 evaluated at Eros.

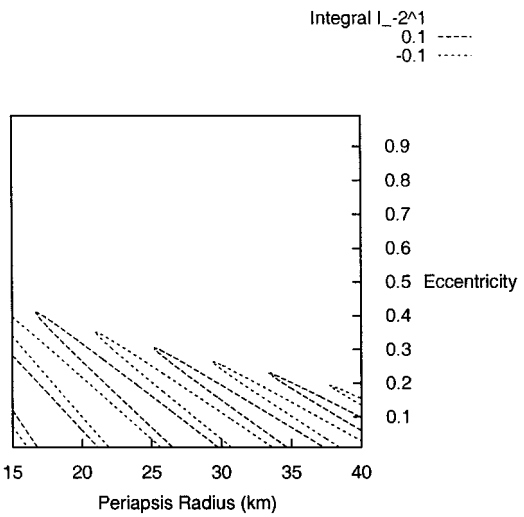

Fig. 2 Contour plot of integral I_{-2}^1 evaluated at Eros.

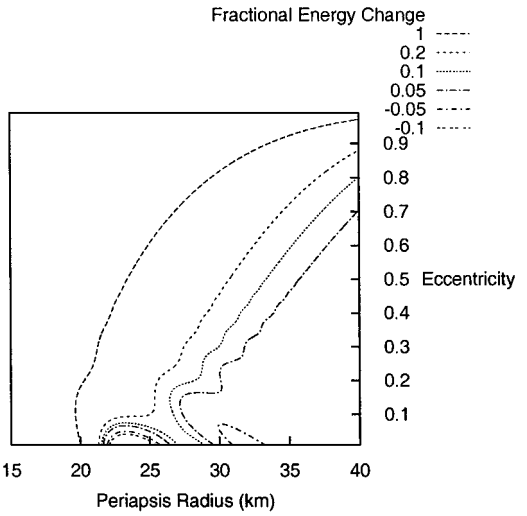

Fig. 3 Contour plot of fractional change in Keplerian energy per orbit, computed specifically for Eros.

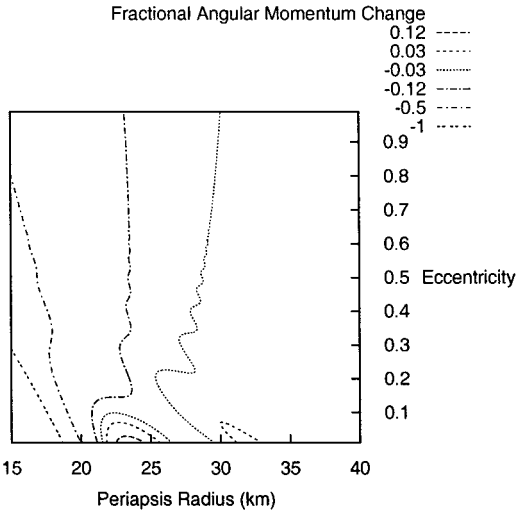

Fig. 4 Contour plot of fractional change in angular momentum per orbit, computed specifically for Eros.

In Figs. 3 and 4 we present contour plots of the fractional change in orbit energy and angular momentum per orbit, using the appropriate Eros constants. These contours are computed using only the I_2^1 integrals, per the preceding discussion. Thus, each of the contours will scale as $\cos^4(i/2)\sin[2(\omega+\Omega)]$, allowing the results to be generalized to a range of orbit inclinations and body-relative geometries (recall that the argument of periapsis and longitude of the ascending node define the location of periapsis in the body-fixed frame). Using this result we can qualitatively predict the expected perturbation experienced by an orbit and use this to compute acceptable limits for proximity operations.

There are many applications of these formulas, including the setting of limits for the minimum periapsis of a spacecraft orbit and the design of very close passes over the asteroid. Related formulas have been used to design relatively safe close flybys over the Eros surface.[22] In that application the functions are used to predict which surface flybys will cause the spacecraft apoapsis and period to increase, ensuring ample time following a close flyby to transition the orbit into a safe orbit at a sufficient distance from the asteroid.

IV. Phase Space Characterization

Next we consider explicit characterizations that can be made concerning the phase space about a uniformly rotating asteroid. These characterizations consist of applications of the Jacobi integral and the explicit computation of families of periodic orbits and their stability about the asteroid.

A. Stability Against Impact

Perhaps the most common application of the Jacobi integral to dynamic systems is found in the restricted three-body problem where it is used to define the zero-velocity curves (cf. Ref. 23). We will make a similar application here. The zero-velocity curves of the current system are found by computing the contours of the gravity plus centripetal potential in the body-fixed position space x, y, and z, where J denotes a particular value of the Jacobi constant. These contour lines then define the limits of physical motion that a spacecraft can have in the body-fixed space, given that value of the Jacobi constant. In general, the spacecraft dynamics must satisfy the inequality constraint

$$U + \tfrac{1}{2}\omega_T^2(x^2 + y^2) + J \geq 0 \tag{31}$$

which constrains the spacecraft to lie on one side of the zero-velocity curves. Figure 5 shows the zero-velocity curves corresponding to the Eros shape model.[3–5] A silhouette of Eros is also shown.

For the purpose of characterizing spacecraft dynamics about this body, we are primarily interested in finding the value of the Jacobi constant such that, for all values of J less than this, the zero-velocity curves are guaranteed to separate the trajectory space containing the asteroid and the space not containing the asteroid. Then we have explicitly that a spacecraft in orbit in the outer region with the appropriate Jacobi integral value can never, under gravitational dynamics alone, impact onto the asteroid surface. For the Eros shape model, this value of J is found to be $J_0 = -5.109 \times 10^{-5}$ km^2/s^2. To ensure stability against impact, we must choose the initial spacecraft conditions such that the spacecraft position resides in the outer portion of the zero-velocity curve and that the value of the Jacobi integral is less than or equal to J_0:

$$C - \omega_T H - R \leq J_0 \tag{32}$$

which provides a simple check in terms of osculating orbital elements for whether or not the spacecraft might impact with the surface at some point in the future. This relation can be expressed in terms of initial osculating elements for an assumed direct, equatorial orbit specified by its periapsis radius, eccentricity, and initial longitude λ in the body-fixed frame:

$$-\mu(1 + e)/2r_p + \omega_T\sqrt{\mu r_p(1 + e)} + U(r = r_p, \lambda) + J_0 = 0 \tag{33}$$

where the force potential U is evaluated from the actual gravity field. Figure 6 shows a plot of the limiting stability against impact curve for the Eros system (including the full effect of the gravity field) in terms of initial periapsis radius and eccentricity for an equatorial orbit. Initial orbits to the left of the line in Fig. 6 may impact with Eros at some point in the future, orbits to the right of this line will not impact with Eros.

What we find from this analysis is that direct, circular orbits must lie outside of 34 km from Eros to not be able to impact on the surface. Note that this does not mean that the spacecraft will not undergo large perturbations and changes in its orbit from the gravity field.

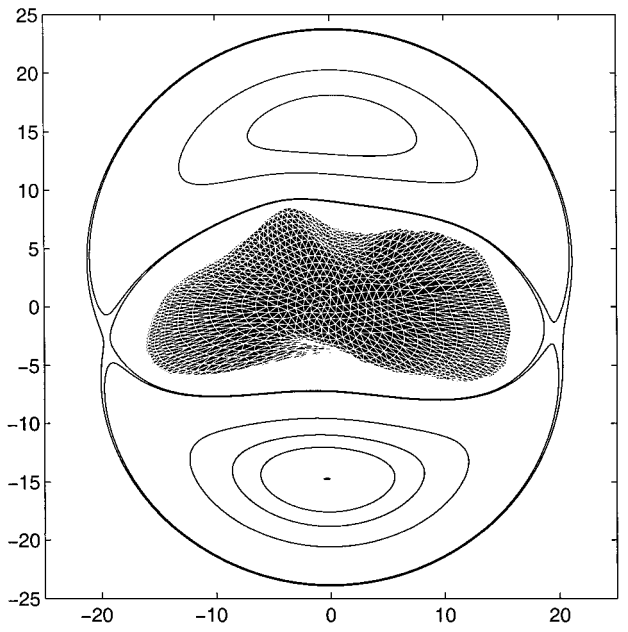

Fig. 5 Zero-velocity curves about Eros projected into the x–y plane.

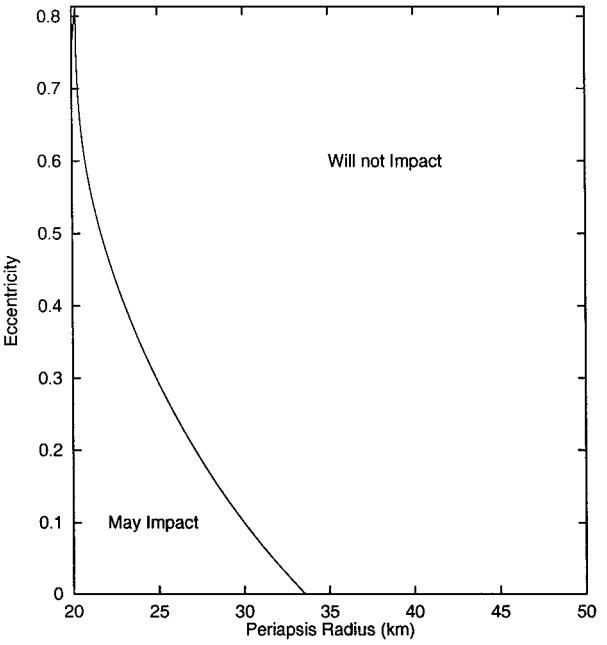

Fig. 6 Stability against impact curve for equatorial, direct orbits.

B. Periodic Orbit Characterizations

Another approach to the stability characterization of orbits about an asteroid is to study the stability of periodic orbit families about the body. If families of periodic orbits can be found that lie near orbits of interest, then the stability of the periodic orbits (something that is easily computed) can be directly related to the expected stability properties of the neighboring orbits. We will consider some basic families of periodic orbits and will concentrate most of our discussion on their geometrical limits for stability. In this context, the existence of a stable orbit will imply that a spacecraft placed near such an orbit will not experience large changes in its orbital elements over time spans of interest, usually days to weeks. An unstable orbit implies that, depending on the characteristic time of the instability, the spacecraft may deviate markedly from the original trajectory in a fairly short time. The characteristic instability times of orbits about asteroids can be rather short and may interfere with orbital operations. This is especially true when one considers the navigation of spacecraft because flying in an unstable orbit environment implies that the orbit uncertainty becomes stretched at a hyperbolic rate, leading to greater uncertainties of where the spacecraft is.[24]

First we discuss computational issues for periodic orbits and some special resonance properties that these orbits have. Then we discuss synchronous orbits, direct equatorial periodic orbits, and retrograde equatorial periodic orbits. A few comments on the stability of out-of-plane orbits are also given.

1. Computational Issues

The traditional approach to analytical or numerical computation of periodic orbits relies heavily on the symmetric properties of the forces in the system. Examples of this include the computation of periodic orbits in the restricted three-body problem and the Hill problem, best exemplified by the seminal work of Hénon (see Ref. 23). This approach has also been used to compute symmetric periodic orbits about triaxial ellipsoids.[3] For application to real objects, however, there are no symmetries in the force fields, and the periodic orbit computation must be generalized to a form that does not rely on such symmetries.

The approach is an application of the Poincaré map with the surface of section chosen to be normal to a convenient surface in phase space, generally chosen to correspond to a position $\boldsymbol{r}_l = c$. Where $\boldsymbol{r}_l$ is a position coordinate in Cartesian space, l equals 1, 2, or 3, and c is a constant value that the trajectory passes through each orbit (often taken to be equal to zero). The Poincaré map is then defined as the map from one (transversal) crossing of the surface $\boldsymbol{r}_l = c$ to the next. The transversal condition needed for the Poincaré map definition is guaranteed by requiring that $\dot{\boldsymbol{r}}_l \neq 0$ whenever $\boldsymbol{r}_l = c$. With this definition, including the conservation of the Jacobi integral, it is possible to remove the two variables $\boldsymbol{r}_l$ and $\dot{\boldsymbol{r}}_l$ from consideration, creating a four-dimensional map from the Poincaré surface to itself.

To extend this map to its first linear variation, we first compute the state transition matrix (STM) along the nominal trajectory, which takes the full six-dimensional state from the first surface crossing to the next surface crossing. We denote the matrix as Φ_{ij}, $i, j = 1, 2, \ldots, 6$, where i denotes the row and j denotes the column of the matrix. For a time-invariant dynamic system (such as our uniformly rotating asteroid), a closed trajectory will have two unity eigenvalues that causes the STM to be useless in converging on a fixed point (which corresponds to a periodic orbit in this system). To create the 4×4 monodromy matrix for this general situation we must remove the two unity eigenvalues from the system. The procedure for doing this is described next.[25]

To create the lower dimensional map, we first constrain the linear variation to lie completely on the Poincaré surface. For the initial linear state, this is easily enforced by setting $\delta \boldsymbol{r}_l(0) = 0$. After the first return, which takes a nominal time T, the l coordinate is not necessarily zero:

$$\delta \boldsymbol{r}_l(T) = \sum_{j=1,\neq l}^{6} \Phi_{lj}\, \delta \boldsymbol{x}_j(0)$$

where $\delta \boldsymbol{x}_i = \delta \boldsymbol{r}_i$, $i = 1, 2, 3$, and $\delta \boldsymbol{x}_{i+3} = \delta \dot{\boldsymbol{r}}_i$, $i = 1, 2, 3$. To force the first return of $\delta \boldsymbol{r}_l$ to be zero requires that the time of first return vary linearly with the initial state:

$$\delta \boldsymbol{r}_l(T + \delta T) = \sum_{j=1,\neq l}^{6} \Phi_{lj}\, \delta \boldsymbol{x}_j(0) + \dot{\boldsymbol{r}}_l(T)\, \delta T \tag{34}$$

Because of the transversality assumptions, this relationship can be solved for the value of time δT, which forces the linear variation of the first return to lie on the Poincaré surface:

$$\delta T = -\frac{1}{\dot{\boldsymbol{r}}_l(T)} \sum_{j=1,\neq l}^{6} \Phi_{lj}\, \delta \boldsymbol{x}_j(0) \tag{35}$$

The linear variation about the Poincaré map then becomes

$$\Phi_{ij}(T) - [\dot{\boldsymbol{x}}_i(T)/\dot{\boldsymbol{r}}_l(T)]\Phi_{lj}(T), \qquad i, j = 1, 2, \ldots, 6, \neq l \tag{36}$$

and is formally a 5×5 linear map that conforms to the Poincaré surface.

Because our system has a Jacobi integral defined for it, one more dimension may be removed to reduce it to a 4×4 map. The monodromy map corresponds to the linear map with no variations in the Jacobi integral value.[23] For our Lagrangian system, this condition is simply stated as a single linear equation:

$$0 = \sum_{j=1}^{3} \frac{\partial J}{\partial \dot{\boldsymbol{r}}_j}\, \delta \ddot{\boldsymbol{r}}_j + \sum_{j=1,\neq l}^{3} \frac{\partial J}{\partial \boldsymbol{r}_j}\, \delta \dot{\boldsymbol{r}}_j \tag{37}$$

where the Jacobi integral was defined in Eq. (8) and we note that $\partial J / \partial \dot{\boldsymbol{r}}_j = \dot{\boldsymbol{r}}_j$ for our system. Again, given our transversality assumption, this variation can be solved for the initial variation in the speed normal to our Poincaré surface:

$$\delta \dot{\boldsymbol{r}}_l = -\frac{1}{\dot{\boldsymbol{r}}_l} \left[\sum_{j=1,\neq l}^{3} \frac{\partial J}{\partial \dot{\boldsymbol{r}}_j}\, \delta \ddot{\boldsymbol{r}}_j + \sum_{j=1,\neq l}^{3} \frac{\partial J}{\partial \boldsymbol{r}_j}\, \delta \dot{\boldsymbol{r}}_j \right] \tag{38}$$

Applying this constraint at the initial variation (at $t = 0$) ensures that the entire linear map has the same value of the Jacobi integral. Application of the constraint eliminates the linear variation of $\delta \dot{\boldsymbol{r}}_l$ as a free parameter, giving us only four independent parameters that can be varied. Also, because the final mapped linear variation must conform to this constraint, one of the final variables can be eliminated from the map because it is redundant given the Jacobi integral constraint; for convenience we remove the final variation of $\delta \dot{\boldsymbol{r}}_l$ from the map. Reduction of these terms yields the final form of our monodromy matrix:

$$\Phi_{ij}(T) - \frac{\dot{\boldsymbol{x}}_i(T)}{\dot{\boldsymbol{r}}_l(T)} \Phi_{lj}(T) - \frac{1}{\dot{\boldsymbol{r}}_l(0)} \left[\Phi_{i(l+3)}(T) - \frac{\dot{\boldsymbol{x}}_i(T)}{\dot{\boldsymbol{r}}_l(T)} \Phi_{l(l+3)}(T) \right] \frac{\partial J}{\partial \boldsymbol{x}_j}(0)$$

$$i, j = 1, 2, \ldots, 6, \neq l, l+3 \tag{39}$$

These reductions remove the unity eigenvalues that exist for any closed trajectory (periodic orbit) in a time invariant system and allow the reduced map to be used to iteratively solve for the fixed points of the map that correspond to the closed periodic orbits. Analyzing the eigenvalues of the 4×4 monodromy matrix also provides details on the stability of the periodic orbits in question.

Given a single periodic orbit computed using the monodromy matrix in Eq. (39) it is possible to generate an estimate of the initial conditions of a neighboring orbit at a slightly different value of Jacobi constant. Following a general procedure,[23] we compute the linear correction to a given fixed point for a fixed point with a slightly different energy:

$$\delta \boldsymbol{x} = (I - A)^{-1} \frac{\partial \boldsymbol{x}_0}{\partial J} \delta J \tag{40}$$

where the monodromy matrix A has its generic unity eigenvalues removed, making the preceding inversion nonsingular for most cases, and the partial of the Poincaré map with respect to the Jacobi integral value is computed assuming a variation in the speed transverse to the Poincaré surface $\dot{\boldsymbol{r}}_l$ only. These approaches allow periodic orbits to be computed and continued numerically in generic, nonsymmetric gravity fields as found at asteroids.

2. Resonances in Periodic Orbits

Other than equilibrium points, all other periodic orbits in the Eros-fixed frame have a definite period of motion and have a nonconstant trajectory about the body. A distinction is made between periodic orbits in the body-fixed frame and in the inertial frame. In general, a periodic orbit in the body-fixed frame will not be a periodic orbit in the inertial frame. However, at special values of the body-fixed orbit period, the periodic orbit will correspond to a periodic orbit in the inertial frame. This situation often corresponds to the intersection of two body-fixed periodic orbit families and usually corresponds to the onset of instability for one of these families. Thus, it is of interest for us to understand the conditions for these resonances to occur in our particular case.

Consider an orbit that repeats itself in the body-fixed space every time period T_P. If we consider this same orbit, now specified in terms of osculating orbit elements, it is clear that the orbit elements (a, e, i) must repeat with period T_P, and the orbit elements of ω and M_0 must shift by some value $2\pi m$, where $m = 0, \pm 1, \pm 2, \ldots$, over a time T_P. The longitude of the ascending node, Ω, need not repeat and instead will shift by a multiple of 2π plus an added angle $\theta = \omega_T T_P$, where ω_T is the rotation rate of the asteroid. Thus, when

this angle θ is commensurate with 2π, the body-fixed periodic orbit is also an inertial periodic orbit, and in the vicinity of such orbits we may expect to find unstable orbit behavior. This is not a necessary condition for instability; as we shall see, orbits may also become unstable when there are no such primary resonances.

Let us consider the two special cases of direct and retrograde periodic orbits. For each of these, the body-fixed period is approximately

$$1/T_P = 1/T_r \pm 1/T_0 \tag{41}$$

$$T_0 = \left(2\pi r^{\frac{3}{2}} \Big/ \sqrt{\mu}\right)\left(1 + 3C_{20}\left|\ 4r^2\right.\right) \tag{42}$$

where the + sign is for retrograde orbits and the − sign is for direct orbits, T_r is the rotation period of the asteroid, and T_0 is the inertial orbital period of the spacecraft (computed with C_{20} corrections and assuming a circular orbit). The direct orbit period has a singularity when the inertial orbit period approaches the body rotation period, corresponding to the equilibrium points and the surrounding phase space. In Fig. 7 we show the ratio of the direct body-fixed orbit period over the Eros rotation period, assuming the described formula. Plotted is the predicted ratio (found using oblate planet theory) and the numerically computed ratio for the direct family of periodic orbits (split into stable and unstable portions of the family). We note commensurabilities of 3:2 at a 35-km radius, 2:1 at a 27.5-km radius, and higher commensurabilities as the singularity is approached. In Fig. 8 we show the ratio of the retrograde body-fixed orbit period over the Eros rotation period, again assuming the preceding formula. The predicted ratio and numerically computed ratio are shown as in Fig. 7. The only significant commensurability is a 1:2 ratio at a radius of approximately 18 km. We shall see, later, that the retrograde orbit becomes unstable in the vicinity of this ratio. The direct orbit instabilities, however, are not as clearly linked to the commensurabilities. This is understood in the context of our analytical discussion, however, which shows that the orbit perturbations felt by the spacecraft orbit can become so large as to overwhelm the effects of resonances.

3. *Equilibrium Points*

A uniformly rotating asteroid with an approximately ellipsoidal shape will in general have four synchronous orbits about it, or four equilibrium points.[3] These points will lie, approximately, along the long and short axes of the asteroid, close to the ideal synchronous orbit radius $r_s = (\mu/\omega_T^2)^{1/3}$, which equals 16.581 km for Eros. Generally, the equilibrium points along the long axis of the body will lie outside of r_s and will always be saddle points, having a hyperbolic stable and unstable manifold and two oscillatory modes (in- and out-of-plane).

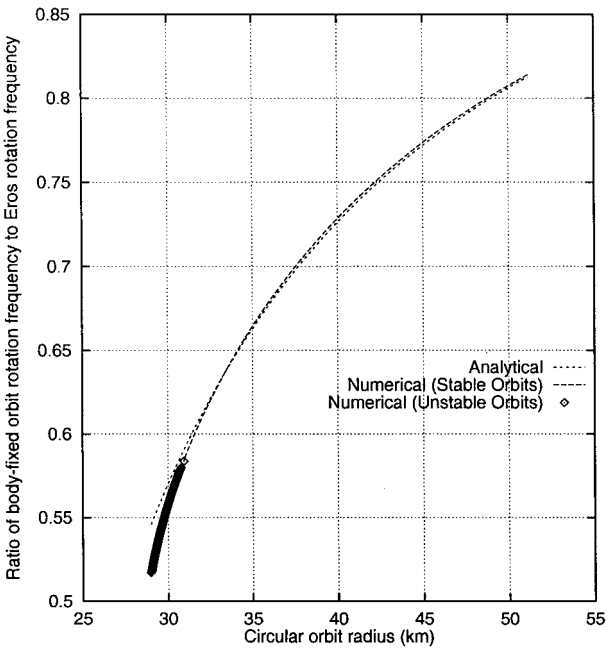

Fig. 7 Ratio of the periodic orbit frequency over the Eros rotation frequency for the direct family of orbits.

Table 1 Positions, stability characteristics and Jacobi constant values for the Eros synchronous orbits

x, km	y, km	z, km	τ, h	J, (km/s)^2
19.546	0.364	−0.839	0.69	-5.103×10^{-5}
−19.600	−0.158	−1.170	0.70	-5.109×10^{-5}
0.106	15.284	0.234	1.59	-4.279×10^{-5}
−0.110	−15.281	0.162	1.64	-4.279×10^{-5}

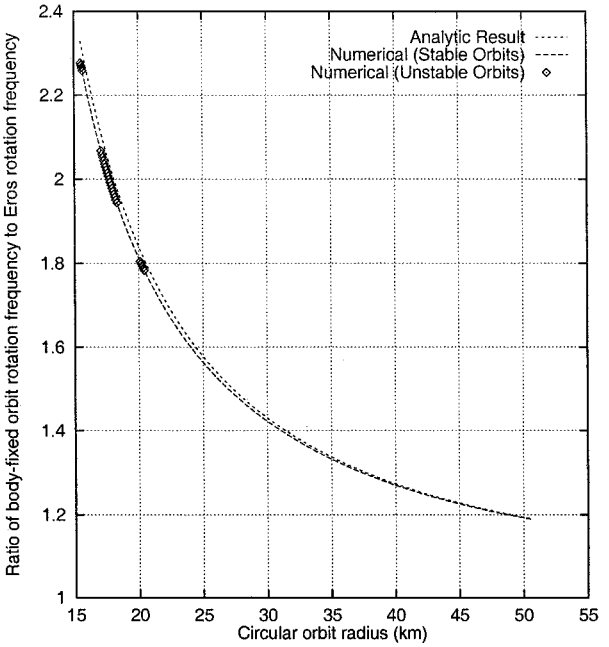

Fig. 8 Ratio of the periodic orbit frequency over the Eros rotation frequency for the retrograde family of orbits.

The equilibrium points along the short equatorial axis will lie inside of r_s and may either be completely oscillatory or have complex roots, leading to a hyperbolic stable and unstable spirals. Specific criteria for the asteroid to have oscillatory or unstable equilibrium points have been developed,[3] and specific examples for realistic shapes have been computed.[4,5] For most asteroid shapes considered thus far, these equilibrium points are usually unstable. Exceptions will occur if the body has a small shape ellipticity in the equator, rotates slowly, or has a large density.

For the Eros shape model in question, we compute the four synchronous orbits (all unstable) and present their coordinates as well as their characteristic times and Jacobi values in Table 1.

We note that the smallest value of J for the equilibrium points, -5.109×10^{-5}, serves as the constant for the stability against impact criterion developed earlier.

In terms of the osculating elements of such an equilibrium point, we note that they are all constant (evident given that the period of motion is effectively zero) except for the longitude of the ascending node, which has a secular rate equal to the rotation rate of the asteroid.

4. *Direct Periodic Orbits*

The family of direct, equatorial, near circular, body-fixed periodic orbits were computed about this model of Eros. Figure 7 shows the family as a curve between mean orbit radius and orbit period frequency divided by Eros rotation frequency. Far from the body these orbits are stable, as expected; however, as the family comes closer to the body they become unstable. For the circular branch of the family this occurs at a radius of approximately 30.8 km and a Jacobi integral value of -4.938×10^{-5}. Before this stability bifurcation occurs, the family itself splits into a circular branch and two elliptic

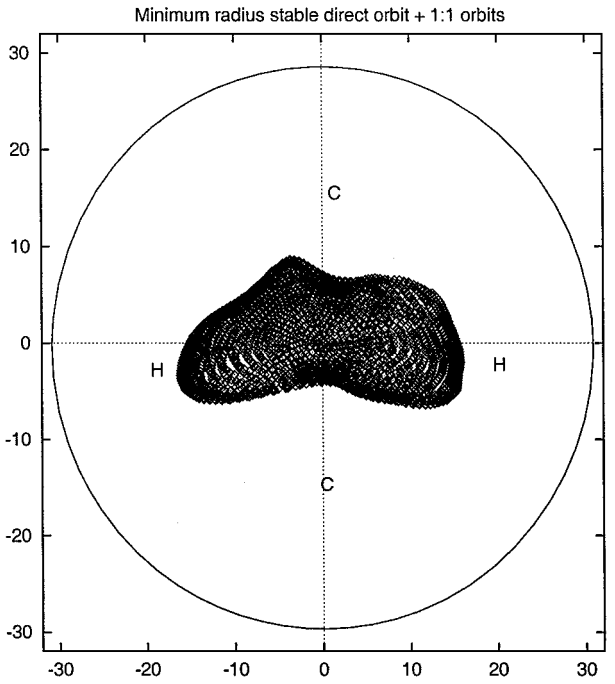

Fig. 9 Minimum radius stable, direct circular orbit about Eros and locations of the unstable 1:1 synchronous orbits projected into the x–y plane.

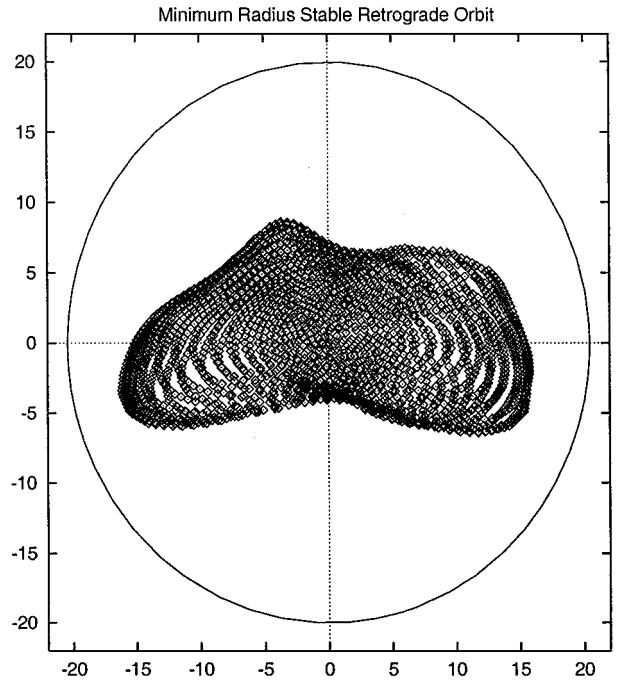

Fig. 10 Minimum radius stable, retrograde circular orbit about Eros projected into the x–y plane before the first instability interval is encountered.

branches; the elliptic branches lose their stability at a slightly higher value of the Jacobi constant.

The proper interpretation of this result is that the minimum stable orbital radius about Eros will be ~31 km, but this assumes some fairly special initial conditions. It is possible, at higher radius values, to find nonperiodic orbits that are characterized by having finite Lyapunov characteristic exponents (indicating that they are unstable). Thus, this limit should be considered to be an absolute minimum for stable, direct, equatorial orbits about Eros. Note that this minimum orbit radius violates the stability against impact limit implying that, if sufficiently perturbed from its stable orbit, it is possible for the spacecraft to impact on the asteroid surface.

It is significant to note from Fig. 7 that the onset of instability is not associated with any particular resonance, leading us to conclude that it is associated with the increasing strength of the gravity perturbations as the direct orbit draws closer to the rotating body and its C_{22} gravity term. Observing the predicted fractional change in orbit energy and angular momentum in the vicinity of where the periodic orbits first become unstable in Figs. 3 and 4, we note that the fractional change in each of these quantities is on the order of 3–5%, leading us to conclude that perturbations of this magnitude may destabilize the orbit dynamics. Shown in Fig. 9 is the minimum radius, direct, stable circular orbit about Eros and the 1:1 synchronous orbits, all projected into the x–y plane. Also shown is a silhouette of Eros.

5. Retrograde Orbits

Periodic orbits are also computed that lie in the equatorial plane but travel in the opposite sense of the asteroid rotation. Figure 8 presents the orbit radius–frequency ratio curve for this orbit family. Generally speaking, such retrograde orbits are stable at almost all radii, even close to the asteroid surface. The reason for this stability is easy to understand: When orbiting in the opposite sense of the asteroid rotation, the destabilizing effect of the C_{22} gravity term is diminished because its effect becomes averaged out in space due to the large relative angular motion between the spacecraft and asteroid. In fact, as the spacecraft orbit becomes close to the asteroid, its rotation rate increases, and, hence, the effective variations of the asteroid's gravity field diminish. This is clearly evident when numerically integrated retrograde orbits are compared with predictions from modeling the ellipsoid as an oblate body.[3] For retrograde orbits, we see that this comparison holds up quite well, indicating that these orbits are stable. This fact is used in the nominal design of the Eros orbital operations[4] and allows the NEAR spacecraft to come close to the Eros surface.

There are, however,[22] some notable exceptions to this stability. These occur when resonances develop between the asteroid rotation rate and the secular motion of the spacecraft orbits' longitude of ascending node (as discussed earlier). For the case of Eros, we see that these resonances should occur in the vicinity of 18 km, where a 1:2 commensurability exists between the periodic orbit period and the asteroid rotation rate. We also note an isolated instability region around 20 km, corresponding to the intersection of the retrograde orbits with an out-of-plane family of orbits with twice the period. This result is not specifically predicted by the inertial resonance relations and is due to more complex interactions occurring in the phase space. Shown in Fig. 10 is the minimum radius, retrograde stable circular orbit about Eros, projected into the x–y plane, before the first instability interval is encountered. Also shown is a silhouette of Eros.

Based on these instability limits, a reasonable constraint to place on retrograde, equatorial orbits is that they lie outside of 21 km from the center of Eros. Again, the danger of flying in or near a region of unstable orbits is due both to the possibility that the orbit may diverge from its nominal path and that the orbit uncertainty will increase significantly.

C. Out-of-Plane Orbits

The analysis thus far has focused on orbits in or near to the asteroid equatorial plane. When significantly out-of-plane orbits are considered, several difficulties arise. For the periapsis and node arguments to have their required resonance, there are more stringent constraints placed on the orbit period so that, physically, the spacecraft is in the equatorial plane after one or more rotations of the central body. This restriction means that out-of-plane periodic orbits do not exist at all radii as the equatorial families do, and thus are less useful in analyzing the stability of general motions about the asteroid.

To gain some insight into the stability of polar (or higher inclination) orbits we combine earlier analysis results from the stability limit of direct periodic orbits with the analytical results found earlier for the change in energy and angular momentum. Let us consider, for definiteness, the stability of a polar orbit ($i = 90$ deg), leading to a scaling factor for the contour plots of $\cos^4(\pi/4) = 0.25$. Thus, we must scale the contour plot by one-quarter. Because of differences

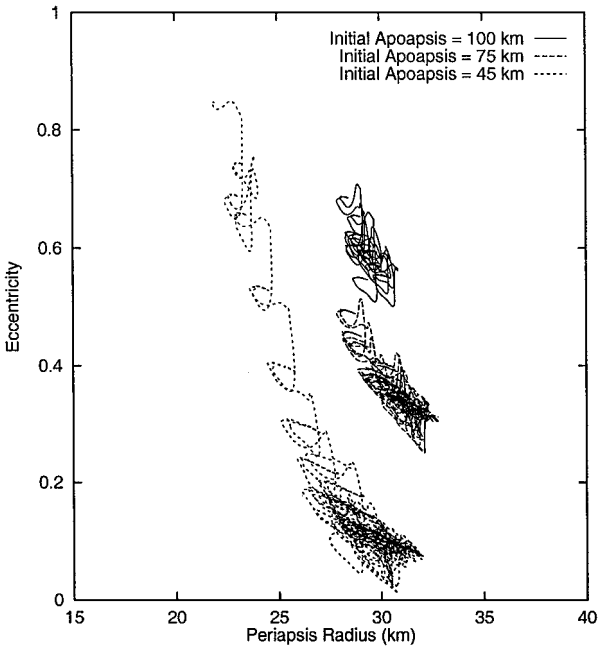

Fig. 11 Periapsis radius–eccentricity plots of three polar orbits over 600 h (25 days); note the diffusion of the trajectories over time.

in the gravitational and orbit interaction for a polar orbit (the interactions are more varied because there are more possible encounter geometries when in the nominal orbit) a reasonable criterion for stability appears to occur when the changes in orbit energy and angular momentum are on the order of 1%. This corresponds to the 5% contour lines on Figs. 3 and 4 and gives an indication of reasonable stability limits for polar orbits.

The actual dynamics of polar (or of any) orbits about such a body are quite interesting. Because of the quasi-random movement of the argument of periapsis and longitude of the ascending node in the body-fixed space, the changes in energy and angular momentum will either add or subtract to the orbit, introducing the possibility of an orbit having random walks in terms of orbit elements. Figure 11 shows three numerically integrated polar orbits, started with an initial periapsis radius of 30 km and apoapsis radii of 45, 75, and 100 km, respectively. Each is integrated for 600 h (25 days), and their trajectory in the periapsis radius–eccentricity space is plotted. Figure 11 shows how individual trajectories can either be confined to regions of orbit element space or diffuse into escaping or impacting trajectories. Whereas there is significant correlation between Fig. 11 and Figs. 3 and 4, the controlling dynamic issues are also evidently much deeper. Current research is attempting to further understand the relation between the analytical formulas and numerical integrations.

V. Conclusions

This paper presents a set of systematic computations and analyses that parameterize the orbit dynamics that a spacecraft will be subject to while in orbit about a uniformly rotating asteroid or comet. Such a set of computations is useful for any and all orbital missions to small bodies, as the specific size, shape, density, and rotation state of those bodies will not be known prior to rendezvous with that body. Once rendezvous occurs, it is imperative that a basic orbital characterization of the body be performed in preparation for the detailed navigation and mission design planning.

The computations provided give us specific limits on stability against impact with the body, approximate formulas to compute changes in orbit Keplerian energy, angular momentum, inclination, period, argument of periapsis, and longitude of ascending node accounting for the body's oblateness and ellipticity. Also, specific methodologies and results for characterizing the orbital space in terms of periodic orbit analysis are given, with specific applications. Significantly, we note that retrograde orbits may become unstable close to the asteroid for some combination of parameters.

The analysis in this paper has been specifically applied to the NEAR spacecraft at the asteroid Eros, using preencounter models of that body. The most significant results of that portion of the analysis is that the minimum radius for a stable, direct, equatorial, circular orbit is approximately 31 km; the minimum radius for a direct, equatorial, circular orbit that cannot impact with the asteroid surface is 34 km; and the minimum retrograde, equatorial, circular orbit radius before instabilities appear is 21 km. Also, contour plots are presented that can be used to delimit regions of orbit element space (periapsis radius and eccentricity to be precise) where perturbations to the spacecraft orbit may become too large. Comparison of stability limits for direct periodic orbits indicate that when orbit energy and angular momentum change by more than ~3% the spacecraft orbit begins to destabilize. This simple criterion can be used to design orbital stability criteria for three-dimensional orbits. Although not completely characterizing the orbital space about the asteroid, these numbers certainly provide the basic framework from which a mission and navigation plan can be generated.

Acknowledgments

The research described in this paper was performed for the Near Earth Asteroid Rendezvous mission Navigation Team under a contract with the Jet Propulsion Laboratory, California Institute of Technology. Partial support of D. J. Scheeres was also given by NASA's Planetary Geology and Geophysics Program.

References

[1]Scheeres, D. J., Ostro, S. J., Hudson, R. S., DeJong, E. M., and Suzuki, S., "Dynamics of Orbits Close to Asteroid 4179 Toutatis," *Icarus*, Vol. 132, No. 1, 1998, pp. 53–79.

[2]Chauvineau, B., Farinella, P., and Mignard, F., "Planar Orbits About a Triaxial Body: Application to Asteroidal Satellites," *Icarus*, Vol. 105, No. 2, 1993, pp. 370–384.

[3]Scheeres, D. J., "Dynamics about Uniformly Rotating TriAxial Ellipsoids: Applications to Asteroids," *Icarus*, Vol. 110, No. 1, 1994, pp. 225–238.

[4]Scheeres, D. J., "Analysis of Orbital Motion Around 433 Eros," *Journal of Astronautical Sciences*, Vol. 43, No. 4, 1995, pp. 427–452.

[5]Scheeres, D. J., Ostro, S. J., Hudson, R. S., and Werner, R. A., "Orbits Close to Asteroid 4769 Castalia," *Icarus*, Vol. 121, No. 1, 1996, pp. 67–87.

[6]Scheeres, D. J., Marzari, F., Tomasella, L., and Vanzani, V., "ROSETTA Mission: Satellite Orbits Around a Cometary Nucleus," *Planetary and Space Science*, Vol. 46, No. 6/7, 1998, pp. 649–671.

[7]Scheeres, D. J., "The Effect of C_{22} on Orbit Energy and Angular Momentum," *Celestial Mechanics and Dynamical Astronomy*, Vol. 73, No. 1/4, pp. 339–348.

[8]Miller, J. K., Bollman, W. E., Davis, R. P., Helfrich, C. E., Scheeres, D. J., Synnott, S. P., Wang, T. C., Williams, B., and Yeomans, D. K., "Navigation Analysis for Eros Rendezvous and Orbital Phases," *Journal of Astronautical Sciences*, Vol. 43, No. 4, 1995, pp. 453–476.

[9]Burns, J. A., and Safronov, V. S., "Asteroid Nutation Angles," *Monthly Notices of the Royal Astronomical Society*, Vol. 165, 1973, pp. 403–411.

[10]Harris, A. W., "Tumbling Asteroids," *Icarus*, Vol. 107, 1994, pp. 209–211.

[11]Balmino, G., "Gravitational Potential Harmonics from the Shape of an Homogeneous Body," *Celestial Mechanics and Dynamical Astronomy*, Vol. 60, 1994, pp. 331–364.

[12]Werner, R. A., and Scheeres, D. J., "Exterior Gravitation of a Polyhedron Derived and Compared with Harmonic and Mascon Gravitation Representations of Asteroid 4769 Castalia," *Celestial Mechanics and Dynamical Astronomy*, Vol. 65, 1997, pp. 313–344.

[13]Werner, R. A., "The Gravitational Potential of a Homogeneous Polyhedron," *Celestial Mechanics and Dynamical Astronomy*, Vol. 59, 1994, pp. 253–278.

[14]Veverka, J., Thomas, P., Bell, J. F., II, Bell, M., Carcich, B., Clark, B., Harch, A., Joseph, J., Martin, P., Robinson, M., Murchie, S., Izenberg, N., Domingue, D., Hawkins, E., Warren, J., Cheng, A., Dunham, D., Chapman, C.,. Merline, W., McFadden, L., Wellnitz, D., Malin, M., Owen, W., Miller, J., Wlliams, B. G., and Yeomans, D. K., "NEAR's Flyby Reconnaissance of Asteroid 433 Eros: Imaging and Spectral Results," *Science*, Vol. 285, No. 5427, 1999, pp. 562–564.

[15]Werner, R. A., "Spherical Harmonic Coefficients for the Potential of a Constant-Density Polyhedron," *Computers and Geosciences*, Vol. 23, 1997, p. 1071.

[16]Yeomans, D. K., "Physical and Orbital Characteristics of 433 Eros," *Journal of Astronautical Sciences*, Vol. 43, No. 4, 1995, pp. 417–426.

[17]Brouwer, D., and Clemence, G. M., *Methods of Celestial Mechanics*, Academic, New York, 1961, p. 290.

[18]Garfinkel, B., "On the Motion of a Satellite of an Oblate Planet,"

Astronomical Journal, Vol. 63, No. 1274, 1958, pp. 88–96.

[19]Brouwer, D., "Solution of the Problem of Artificial Satellite Theory Without Drag," *Astronomical Journal*, Vol. 64, No. 1274, 1959, pp. 378–397.

[20]Kozai, Y., "The Motion of a Close Earth Satellite," *Astronomical Journal*, Vol. 64, No. 1274, 1959, pp. 367–377.

[21]Kaula, W. M., *Theory of Satellite Geodesy*, Blaisdell, Waltham, MA, 1966, pp. 49–56.

[22]Antreasian, P. G., Helfrich, C. L., Miller, J. K., Owen, W. M., Williams, B. G., Yeomans, D. K., Giorgini, J. D., Dunham, D. W., Farquhar, R. W., McAdams, J. V., and Scheeres, D. J., "Preliminary Considerations for NEAR's Low-Altitude Passes and Landing Operations at 433 Eros," AIAA Paper 98-4397, Aug. 1998.

[23]Marchal, C., *The Three Body Problem*, Elsevier, New York, 1989, pp. 59–62.

[24]Scheeres, D. J., and Hou, Y., "The Dynamics of Uncertainty: Measuring Orbit Knowledge and Quality in Unstable Orbits," AIAA Paper 98-4559, Aug. 1998.

[25]Scheeres, D. J., "Satellite Dynamics About Asteroids: Computing Poincaré Maps for the General Case," *Hamiltonian Systems with Three or More Degrees of Freedom*, NATO ASI Series, Vol. 533, Kluwer Academic, Norwell, MA, 1999, pp. 554–557.